

PAPER • OPEN ACCESS

Heat transfer along the route to chaos of a swaying thermal plume

To cite this article: D Angeli *et al* 2015 *J. Phys.: Conf. Ser.* **655** 012055

View the [article online](#) for updates and enhancements.

Related content

- [Collision dynamics of laser produced carbon plasma plumes](#)
- [Infrared signature modelling of a rocket jet plume - comparison with flight measurements](#)
- [The Communicating Pipe Model for Icy Plumes on Enceladus](#)

Recent citations

- [On the bimodal nature of a confined buoyant plume. Part II: Flow structure echoes in state space](#)
D. Angeli and A. Pagano



IOP | ebooks™

Bringing together innovative digital publishing with leading authors from the global scientific community.

Start exploring the collection—download the first chapter of every title for free.

Heat transfer along the route to chaos of a swaying thermal plume

D Angeli¹, M A Corticelli², A Fichera³ and A Pagano³

¹ Dipartimento di Scienze e Metodi dell'Ingegneria, Università degli Studi di Modena e Reggio Emilia, Via Amendola 2, 42122 Reggio Emilia (Italy)

² Dipartimento di Ingegneria Enzo Ferrari, Università degli Studi di Modena e Reggio Emilia, Via Vivarelli 10, 41125 Modena (Italy)

³ Dipartimento di Ingegneria Industriale, Università degli Studi di Catania, Viale Andrea Doria 6, 95125 Catania (Italy)

E-mail: ¹diego.angeli@unimore.it

E-mail: ²mauro.corticelli@unimore.it

E-mail: ³apagano@diim.unict.it

Abstract. Detailed analyses have been recently reported on the low order dynamics of a thermal plume arising from a horizontal cylindrical heat source concentric to an air-filled isothermally cooled square enclosure, together with those of the related flow structures, in the limit of the 2D approximation. In particular, within the range of $0 < Ra < 3Ra_{cr}$, with Ra_{cr} corresponding to the loss of stability of the stationary buoyant plume, the entire evolution from a periodic limit cycle (P_1) to the birth of chaos through a period-doubling cascade has been fully explored. With this respect, special attention has been given to the window of quasiperiodic dynamics onto a T_2 -torus that is observed to separate the monoperiodic dynamics from the biperiodic dynamics onto a P_1 and a P_2 -limit cycle, respectively. The results of these analyses hint at the bimodal nature of the overall dynamics, in general, and of the subharmonic cascade, in particular, which are still under investigation. Although relevant on a dynamical perspective, a with a main reflection on the laminar-turbulent transition, the observed oscillations appear to be characterised by comparable amplitudes and to be determined by similar evolutions of the flow pattern evolutions, so that their role on the overall heat transfer rate is expected to be marginal. Within this frame, the present study aims at reporting the influence played by the observed dynamics of the thermal plume and of the flow structures on the global heat transfer rate. In particular, the aim is the assessment of the correlation between the Rayleigh number and the average Nusselt number on the cylinder surface, as well as the effect on the latter of the observed series of bifurcations.

1. Introduction

Several studies have addressed the analysis of the thermo-fluid dynamic behaviour of the buoyant flow arising from a horizontal cylindrical heat source confined within a isothermally cooled concentric square cavity. Particular attention has been devoted to the subcritical flows and to steady-state heat transfer, as well as to the first instabilities of the system, both for the limit case of a horizontal line heat source [1] and as a function of the gap width for variable diameter of the heat source [2–6], under the approximation of 2D flow. Similar investigations were also carried out by Bouafia and Daube [7], on an enclosed square-sectioned horizontal cylinder. In



a preliminary study [6] with a main focus on the system dynamics, the authors reported the bifurcation path from stationary to chaotic behaviour undergone by the flow for increasing Rayleigh number values. The study was developed under various geometrical configurations, as defined by the aspect ratio $A = H/L$, i.e. the ratio between the maximum gap height and the length of the side walls. For the cavities with aspect ratio $A = 5$ and $A = 10$, the flow asset and early bifurcations were found to be primarily determined by the formation of Rayleigh-Benard-type rolls above the heat source. These steady-state, multicellular patterns were seen to undergo symmetry-breaking pitchfork bifurcations, eventually leading to periodic states. For $A = 3.3$ and $A = 2.5$ the dynamics were found to be governed by the oscillations of a swaying thermal plume originating around the cylindrical heat source. More detailed analyses were hence reported [8] for the behaviour of the cavity characterised by aspect ratio $A = 2.5$. For this case the observed scenario was found to consist of a period doubling cascade, at the beginning of which a window of quasiperiodic behaviour on a T_2 -torus is found to separate the period-1 (P_1) orbit from the period-2 (P_2) limit cycle. The subharmonic cascade was followed up to the P_{128} -limit cycle, corresponding to the observation of the seventh period doubling. In order to achieve such a result, together with a very high level of refinement of both the discretisation grid and of the time step adopted for the simulations, a thorough scanning of the Rayleigh number range was performed in order to allow the identification of the whole series of bifurcations leading to chaos.

Even though Squire's theorem [9] ensures that, if the domain is significantly larger along the third dimension with respect to the transverse directions, the first instability takes place always on the transverse plane, this is not generally true for successive transitions; hence, the above-described scenario is not expected to be experimentally observable as a consequence of 3D dynamics, which are not accounted for in the adopted 2D numerical model. Nonetheless, the physical relevance of the scenario under consideration was justified taking into account its qualitative similarity with the experimental results of [10, 11], who reported a similar route to chaos for the Rayleigh-Benard cellular patterns within a rectangular cavity and by Labonia and Guj [12], who reported the route to chaos for a thermal plume confined in a large gap air-filled cylindrical annulus. In the latter, in particular, the influence of three-dimensional effects was shown to emerge well above the critical Ra -value of the first Hopf bifurcation and, hence, in [8] it was inferred that the dynamics of a real 3D square enclosure with the concentric cylindrical heat source can be described with sufficient accuracy by the 2D numerical model, at least for a limited range of Ra above the first Hopf bifurcation.

With respect to the origin of the observed dynamics, the results reported in the previous studies hint at the fundamental bimodal structure of the flow. This structure is, in fact, retained by the modal locking characteristic of the sub-harmonic cascade that follows the window of quasiperiodic behaviour, an observation that was further exploited in [13], with a main focus on the initial transitions, at low values of the Rayleigh number, from the P_1 limit cycle to the quasiperiodic T_2 torus, due to a Neimark-Sacker bifurcation, and from the T_2 torus to the P_2 limit cycle, due to a tangent (flip) bifurcation and corresponding to the locking of the two fundamental modes.

Previous considerations are indeed relevant from a dynamical standpoint in that they play a main role at the beginning of the laminar-turbulent transition. Nonetheless, in any of the observed regimes, the two basic modes are characterised by very similar amplitudes and frequencies and appear to be determined by similar evolutions of the flow patterns within the enclosure. Therefore, their alternate occurrence is not expected to produce relevant variations of the overall heat transfer rate. Within this frame, the present study is devoted to reporting the influence on the global heat transfer rate played by the observed dynamics of the thermal plume and of the flow structures. In particular, the aim is the assessment of the correlation between the Rayleigh number and the average Nusselt number on the cylinder surface, as well as the effect on the latter of the observed series of bifurcations.

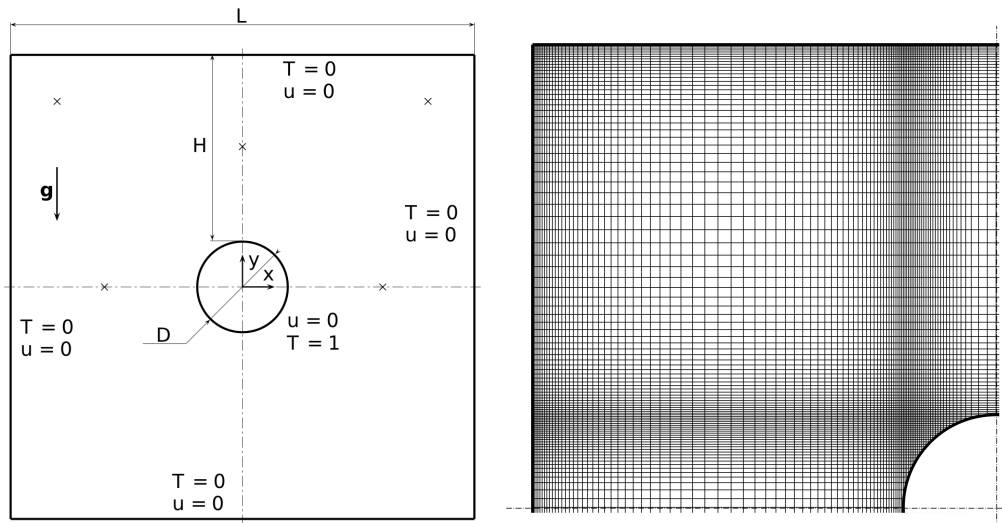


Figure 1. Left: schematic of the system under consideration; (x) symbols indicate locations of the sampling points. Right: quadrant of the computational grid.

2. Problem statement

The problem is stated in terms of the incompressible Navier-Stokes formulation. The Oberbeck-Boussinesq approximation is enforced, all the fluid properties being consistently assumed as constant, apart from density in the buoyancy term.

The governing equations are tackled in their non-dimensional form. The gap between the top of the cylinder and the upper cavity wall is indicated in [5] as the most suitable scale length, $H_{ref} = H$. In fact, it reduces the dependence of the solution ranges on the aspect ratio, in particular, for what concerns the heat transfer rate and the first transitions between different regimes. Moreover, the region above the cylinder is subject to the maximum inverse thermal gradient, *i.e.* to the highest buoyancy force acting on the fluid system, and this is again related to the reference length H .

Temperature is non-dimensionalized according to a reference temperature T_{ref} , *i.e.* the temperature difference between the cylinder and the cavity walls ($T_{ref} = T_S - T_W$), and the following velocity scale is chosen:

$$U_{ref} = \sqrt{g\beta T_{ref} H_{ref}} \quad (1)$$

where g denotes the gravitational acceleration and β is the thermal expansion coefficient of the fluid. The continuity, momentum, and energy equations are given the following form:

$$\nabla \cdot \mathbf{u} = 0 \quad (2)$$

$$\frac{\partial \mathbf{u}}{\partial t} + \mathbf{u} \cdot \nabla \mathbf{u} = -\nabla p + \frac{Pr^{1/2}}{Ra^{1/2}} \nabla^2 \mathbf{u} + T \hat{\mathbf{g}} \quad (3)$$

$$\frac{\partial T}{\partial t} + \mathbf{u} \cdot \nabla T = \frac{1}{(RaPr)^{1/2}} \nabla^2 T \quad (4)$$

where t , \mathbf{u} , p and T represent the dimensionless time, velocity vector, pressure and temperature, respectively, and $\hat{\mathbf{g}}$ is the gravity unit vector. The Rayleigh and Prandtl numbers are defined

as:

$$Ra = \frac{g\beta T_{ref} H_{ref}^3}{\nu\alpha} \quad (5)$$

$$Pr = \nu/\alpha \quad (6)$$

where ν and α represent the momentum and thermal diffusivity, respectively. A constant value $Pr = 0.7$ is assumed for air. With reference to figure 1, the following non-dimensional boundary conditions are imposed:

$$T = 0, \quad \mathbf{u} = \mathbf{0} \quad (7)$$

at the enclosure walls, and:

$$T = 1, \quad \mathbf{u} = \mathbf{0} \quad (8)$$

on the cylinder surface.

3. Numerical methods

The numerical technique adopted is based on a Finite Volume implementation of a second order Projection Method, following [14]. Time-discretizations of the conservation equations are performed according to a three-level scheme, which is fully implicit for the diffusive terms, and explicit Adams-Bashforth for the advective terms. Such a practice is second order accurate in time.

Spatial derivatives are approximated with second order central differences on staggered, non-uniform Cartesian grids. A direct resolution of the discrete momentum and energy equations at each time-step is made possible by means of Approximate Factorization, while the Poisson problem associated with the pressure-velocity coupling [14] is solved through a fast Poisson solver, based on Matrix Decomposition.

The 2D modelling of arbitrarily irregular boundaries on Cartesian grids is achieved thanks to the original scheme developed in [15]. The technique involves a local modification of the 5-point computational stencil where boundary segments intersect the stencil arms. The variables on the modified stencil are mapped on the global grid, by means of a linear operator determined by geometrical features and boundary conditions. The overall accuracy of the method is virtually preserved, as well as the computational efficiency of the Cartesian approach. This represents a significant advantage of the present technique with respect to commercially established, multi-purpose codes. In fact, the possibility of exploiting fast and direct linear solvers for the discrete equations, even in the presence of non-Cartesian boundaries, entails an extremely low computational cost, which made it possible to perform a large number of long-term prediction of a phenomenon which is typically characterised by very long time scales. Furthermore, a direct solution also implies that no artificial perturbation, associated with the residuals of iterative solutions, is applied to the computed flow regime. Finally, the use of Cartesian grids ensures that second-order accuracy is effectively achieved, and this is not always the case with body-fitted, unstructured grids.

The Cartesian grid employed, made up by 190×190 elements, is shown in figure 1. Along both grid directions, a variable spacing was used, and special care was put on the grid sizing of both near-wall areas and internal domain regions, in view of the work objectives. The criteria adopted for the choice of grid spacing and time step size are outlined in detail in [8], while a grid independency test for a periodic flow is reported in [5].

In order to analyze the system dynamics in the vicinity of bifurcation points, Ra was increased monotonically with suitable steps, each simulation starting from the final frame of the preceeding one. All the simulations were protracted until a fixed dimensionless time span was covered, large enough for an asymptotic flow to be attained [8].

Time histories of dimensionless temperature T , and velocity components along x and y directions, respectively u_x and u_y , were tracked for 5 locations, reported in figure 1, in order to be utilized for phase-space representations of the system dynamics.

4. Results and discussion

Table 1 reports the entire sequence of bifurcations driving the flow in the present system from steady-state to chaos; this was determined by Angeli and Pagano [8] by means of an accurate scanning of the range of the bifurcation parameter (i.e. the Rayleigh number) over which the transition occurred. The bifurcation scenario can be well described by a Feigenbaum cascade, at the beginning of which the first doubling of the fundamental oscillation period Π (P_1 flow) is preceded by the occurrence of a window of Ra -values for which the flow is quasiperiodic. For such a flow, the trajectories of state-space variables lie on a T_2 torus, and the system dynamics are completely described by two incommensurate frequencies. The peculiarity of the observed behaviour lies in the fact that the period-2 (P_2) flow emerges from the locking of the secondary frequency of the quasiperiodic flow on the exact half of the primary one. A detailed description of the quasiperiodic dynamics has been reported by the authors in [13]. In the following, the overall features of the oscillating thermal and flow fields will be described, and the influence of successive bifurcations on the overall heat transfer will be discussed.

Figure 2 displays a representation of nine snapshots of the evolution of the temperature field in the system over one period Π of oscillation of the P_1 flow, for $Ra = 110000$. The temperature field is represented by means of pseudo-interferograms: dimensionless temperature values is transformed into fringes which represent successive ranges of the variable. The temperature difference between two successive fringes is $\Delta T = 0.1$. The adopted representation is particularly useful since it implies an analogy with experimental visualizations like the ones presented in [16], and allows for a simple but straightforward identification of the main thermal structures.

From the snapshots, it appears evident that the dominating feature is the swaying thermal plume which rises from the heated cylinder. At the beginning of one oscillation period ($t = 0$), the plume stands upright above the cylinder, but it can be noticed how the thermal field is not symmetric with respect to the vertical axis of the enclosure. The plume then starts to bend towards the right-hand side of the cavity, until it gets closest to the lateral enclosure wall at $t \approx \Pi/4$. Subsequently, the plume reverts back to its central position for $t \approx \Pi/2$: at that time instance, the thermal field is exactly the mirrored image of the field for $t = 0$ with respect to the vertical axis. Then, the plume concludes its oscillation by leaning towards the left-hand

Table 1. Flow regimes and corresponding ranges of Ra throughout the transition to chaos [8].

flow regime		$Ra \times 10^{-5}$
steady-state	S	≤ 0.66200
periodic	P_1	$0.66200 \div 1.73500$
quasiperiodic	T_2	$1.74000 \div 1.79270$
periodic	P_2	$1.79280 \div 1.89750$
periodic	P_4	$1.89800 \div 1.93670$
periodic	P_8	$1.93675 \div 1.94730$
periodic	P_{16}	$1.94735 \div 1.94950$
periodic	P_{32}	$1.94955 \div 1.94990$
periodic	P_{64}	$1.94995 \div 1.95002$
periodic	P_{128}	$1.95002 \div 1.95010$
chaos	N	≥ 1.95025

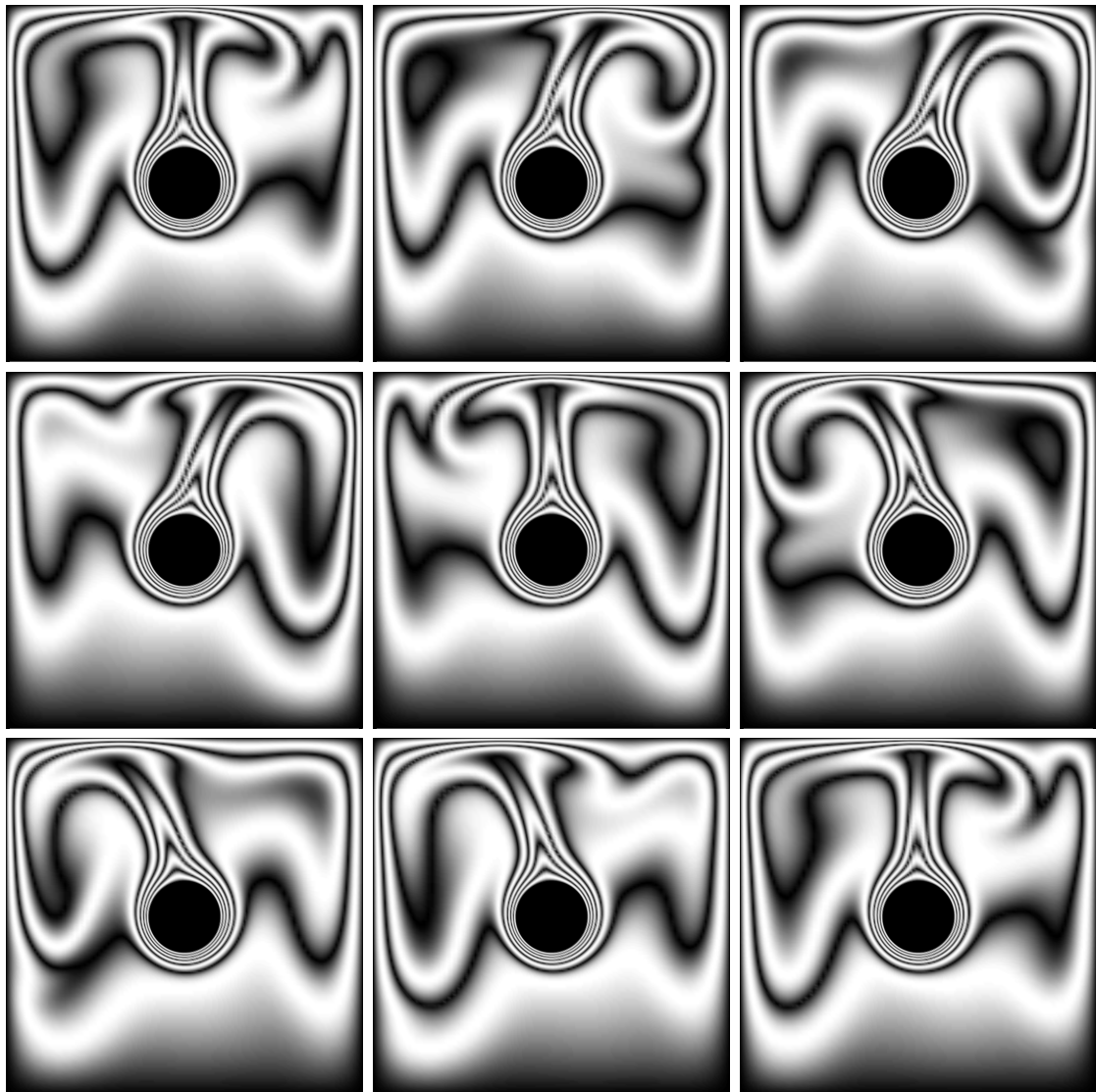


Figure 2. Sequence of pseudo-interferograms portraying the temperature field over one oscillation period Π for P_1 flow at $Ra = 110000$. Each fringe corresponds to a $\Delta T = 0.1$. Time distance between successive snapshots is $\Delta t = \Pi/8$.

cavity wall, and finally returning to the initial position for $t = \Pi$.

Whilst the swaying motion of the plume and its impingement on the enclosure ceiling can be expected to determine large perturbations in the thermal boundary layer of the cavity sidewalls, and a periodic shifting of the peak heat transfer coefficient along the top wall, the boundary layer around the cylinder is observed to be largely uninfluenced by the plume oscillation, with a reduced impact on the time dependence of the Nusselt number along the cylinder itself.

Figure 3 reports a streamline visualization of the flow patterns underlying the temperature fields displayed in Figure 2. The flow field is substantially dominated by the alternate expansion and contraction of two main counter-rotating vortices which alternately sustain the thermal plume. As soon as the plume bends towards the right hand side of the enclosure, the right-hand vortex, which encircles the cylindrical source, contracts, and its center shifts towards the right and the bottom of the cavity. Contemporarily, the left-hand circulation expands and divides in

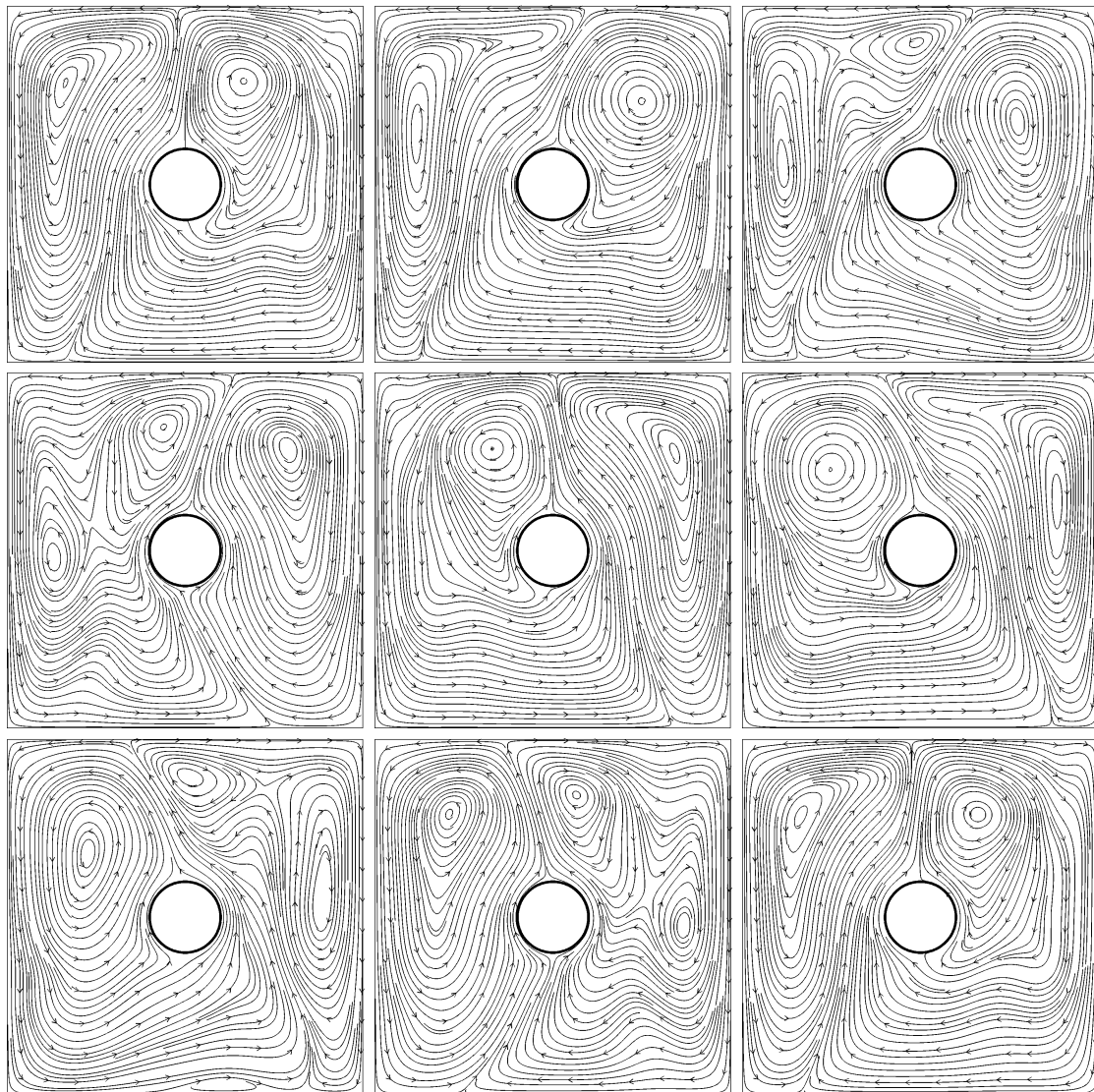


Figure 3. Sequence of streamline visualizations of the flow field over one oscillation period Π for P_1 flow at $Ra = 110000$. Time distance between successive snapshots is $\Delta t = \Pi/8$.

two smaller, distinct cells, which merge back in a bigger circulation when the plume returns in the central position ($t \approx \Pi/2$). The same behaviour, albeit with reversed sides, is observed in the second half of the plume cycle.

For the sake of brevity, analogous visualizations for all the flow regimes listed in Table 1 are not included here. Nevertheless, a close inspection of similar sequences of snapshots collected for the T_2 regime revealed that, coherently with the emergence of two independent frequencies f_1 and f_2 in the power spectra of the state variables [13], two distinct “modes” of oscillation could be singled out. These modes alternate almost every other plume oscillation, the ratio f_1/f_2 between the two frequencies being close to 2, and are characterized by the creation and destruction of smaller flow structures aside from the ones described in Figure 3, appearing in slightly but noticeably different manners for each of the two modes. However, such variations in the flow field appeared as hardly distinguishable in the thermal field, whose main pattern never strays significantly from the one depicted in Figure 2. For this reason, the observed evolution of

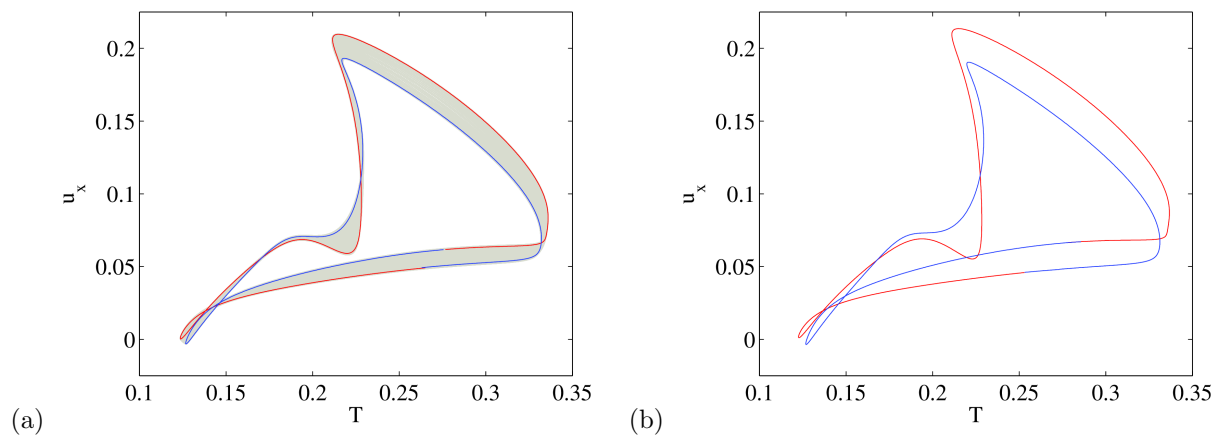


Figure 4. Attractors at point (0.5,0), projected onto the u_x - T state space for (a) T_2 flow at $Ra = 1.76875 \times 10^5$ and (b) P_2 flow at $Ra = 1.8 \times 10^5$. Trajectories corresponding to the primary (red) and secondary (blue) oscillation modes are highlighted.

the flow patterns and system dynamics are expected to produce marginal effects on the overall heat transfer coefficient. Similar considerations could be inferred for the P_2 regime, when the two frequencies lock at $f_1/f_2 = 2$.

A synthetic but effective visualization of the two basic modes can be drawn in the state space spanned by the variables T and u_x , by plotting the trajectory obtained by the time series sampled at point (0.5,0) (see Figure 4). In the quasiperiodic regime (Figure 4a), the two modes can be highlighted as two successive segments of the trajectory which coils itself onto the T_2 torus. In the P_2 regime (Figure 4b), instead, they form the closed curve that corresponds to the period-2 limit cycle. It can be observed how, for both regimes, the two basic modes are characterised by very similar amplitudes and frequencies, and are determined by similar evolutions of the flow patterns within the enclosure. Moreover, in the subsequent period doublings, the two basic modes remain as the dominant patterns, and are recognizable even when the flow is fully chaotic (up to $Ra = 2 \times 10^5$). For this reason, their alternate occurrence is not expected to produce relevant variations of the overall heat transfer rate throughout the whole transition scenario.

To verify the above hypotheses, the entire database of time- and surface- averaged Nusselt number values on the cylinder has been analyzed in terms of the dependence on Ra . and subdivided into four different macro-groups, based on the observed trend. Such groups are listed in Table 2. For each group, a least-squares fitting has been carried out in order to express the $Nu(Ra)$ dependence via a power-law correlation of the following kind:

$$Nu = C Ra^n \quad (9)$$

Table 2. Best-fit coefficients for Equation (9) for different flow types.

flow types		C	n
steady-state flow	S	0.988	0.19
supercritical flow	P_1	1.336	0.16
fully periodic and quasiperiodic flow	$P_1 \rightarrow T_2$	0.847	0.20
phase locking and subharmonic cascade	$P_2 \rightarrow P_4 \rightarrow \dots \rightarrow N$	0.740	0.21
complete transition	$S \rightarrow N$	1.021	0.18

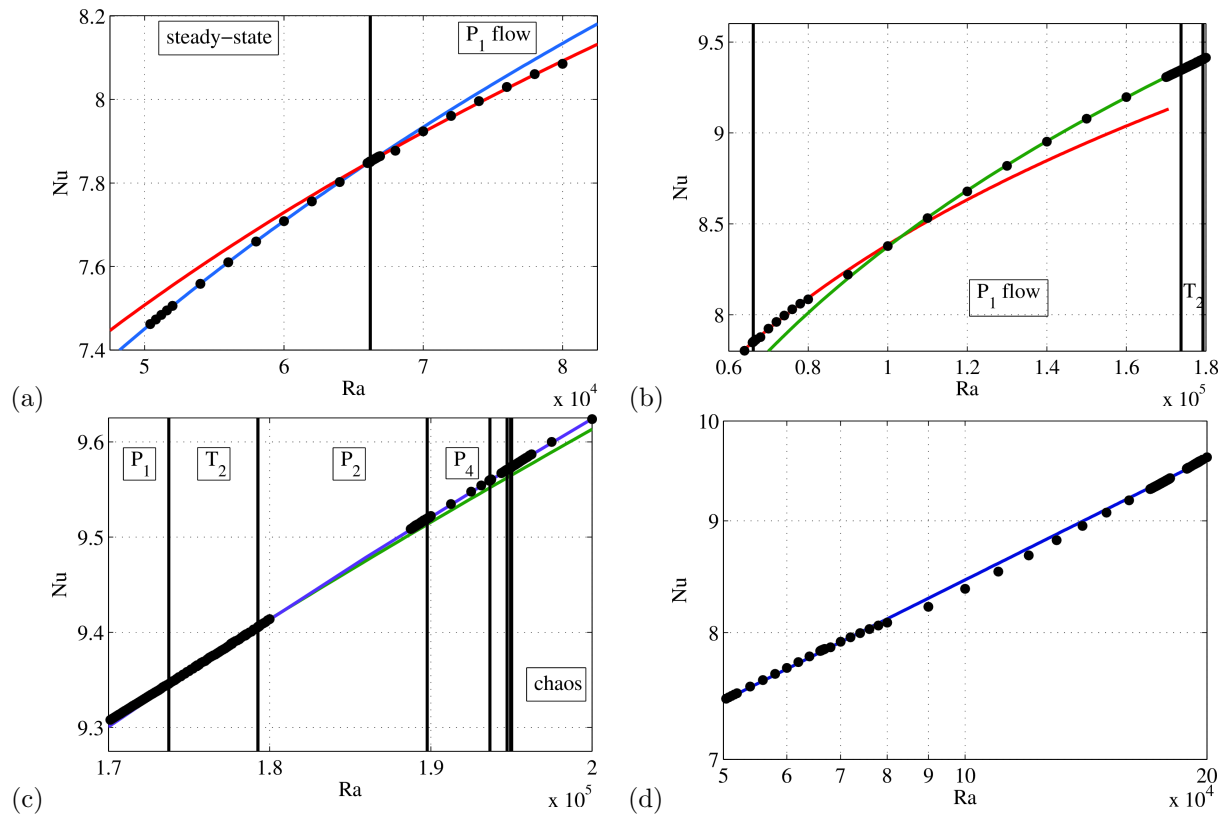


Figure 5. Best-fits (solid lines) and numerical values (dots) of the average Nusselt number on the cylinder for different flow ranges (a)-(c) and for the whole transition range (d).

An additional fitting has been performed for the whole transition range. Such fittings are represented in Figure 5 along with numerical results, in their respective range of interest.

The first variation in the $Nu(Ra)$ dependence can be identified at the transition point between steady-state flow and P_1 flow (Figure 5a), as already suggested in [6]. Quite surprisingly, the second variation occurs in the middle of the P_1 range, around $Ra \approx 10^5$ (Figure 5b): there, the exponent n to be given to Equation (9) $Nu(Ra)$ significantly increases, and remains valid also for the whole T_2 range. Such an unexpected change in behaviour, apparently unlinked with the transitional dynamics, could be due to the full establishment of the regime portrayed in Figures 2 and 3, and to the progressive increase of the oscillation amplitude with Ra with respect to the early stages of the development of the P_1 flow. As long as the T_2 regime disappears, and the period-2 flow emerges, the $Nu(Ra)$ trend changes again, albeit very slightly (Figure 5c). The exponent n increases by a small amount and the observed dependence remains valid up to the chaotic flow regime ($Ra = 2 \times 10^5$).

Figure 5d finally shows the best fit of Equation (9) to the numerical data of the whole transition range: it can be seen how a single exponent is fairly adequate to represent the Nusselt number variation throughout the successive bifurcations. In fact, despite local discrepancies are noticeable (especially in the P_1 range), the maximum deviation of the numerical data from the fit does not exceed 1%, which is indeed a satisfactory accuracy. Hence, it can be concluded that, within the limits of the 2D assumption, the influence of flow transitions on overall heat transfer is not significant.

5. Concluding remarks

Starting from the analysis of an extensive database of numerical simulations already described and discussed in recent works, the influence of successive flow bifurcations on natural convection heat transfer from an enclosed horizontal cylinder was investigated here. In the case under consideration, the scenario leading to chaos consists in a sequence of period-doubling bifurcations, preceded by a window of quasiperiodic flow.

An analysis of the evolution of the system over one oscillation period revealed that the main feature of the thermal field is the swaying motion of the plume forming above the cylinder, while the flow is characterized by the alternate contraction and expansion of two counter-rotating vortices, and the formation of secondary vortices. As Ra increases, two main oscillation modes emerge in the flow fields and persist throughout the whole transition range.

Despite the peculiarity and complexity of the scenario, flow transitions were observed to have a marginal effect on the overall heat transfer, which could be correlated either with different equations considering different intervals of the leading parameter (Ra), only partially related to the bifurcation points, or by a single power-law correlation spanning the entire transition range. The latter matches the numerical data with an accuracy of 1%.

References

- [1] Desrayaud G and Lauriat G 1998 *J. Fluid Mech.* **252** 617–646
- [2] Moukalled F and Acharya S 1996 *Journal of Thermophys.* **10** 524–531
- [3] Shu C and Zhu Y D 2002 *Int. J. Num. Meth. Fluids* **38** 429–445
- [4] Kim B S, Lee D S, Ha M Y and Yoon H S 2008 *Int. J. Heat Mass Transf.* **51** 1888–1906
- [5] Angeli D, Levoni P and Barozzi G S 2008 *Int. J. Heat Mass Transf.* **51** 553–565
- [6] Angeli D, Pagano A, Corticelli M A, Fichera A and Barozzi G S 2011 *Frontiers in Heat and Mass Transfer* **2** 023003
- [7] Bouafia M and Daube O 2007 *Int. J. Heat Mass Transf.* **50** 3599–3615
- [8] Angeli D and Pagano A 2013 *Int. J. Therm. Sci.* **68** 20–31
- [9] Squire H B 1933 *Proceedings of the Royal Society of London. Series A, Containing Papers of a Mathematical and Physical Character* **142** 621–628
- [10] Ecke R E, Mainieri R and Sullivan T S 1991 *Physical Review A* **44** 8103–8118
- [11] Glazier J A and Libchaber A 1988 *IEEE Transactions on Circuits and Systems* **35** 790–809
- [12] Labonia G and Guj G 1998 *J. Fluid Mech.* **375** 179–202
- [13] Angeli D, Corticelli M, Fichera A and Pagano A 2014 *Journal of Physics: Conference Series* **501**
- [14] Gresho P M 1990 *Int. J. Num. Meth. Fluids* **11** 587–620
- [15] Barozzi G S, Bussi C and Corticelli M A 2004 *Numerical Heat Transfer B* **46** 56–77
- [16] Cesini G, Paroncini M, Cortella G and Manzan M 1999 *Int. J. Heat Mass Transf.* **42** 1801–1811